

## Experimental study of heat transfer in the front separation region during the interaction of a supersonic flow with a cylinder

© P.A. Popov,<sup>1</sup> E.V. Kolesnik,<sup>2</sup> N.A. Monachov,<sup>1</sup> A.V. Masyukevich,<sup>1,2</sup> E.V. Babich<sup>2</sup>

<sup>1</sup>Ioffe Institute,

194021 St. Petersburg, Russia

<sup>2</sup>Peter the Great Saint-Petersburg Polytechnic University,

195251 St. Petersburg, Russia

e-mail: pavel.popov@mail.ioffe.ru

Received October 2, 2024

Revised November 3, 2024

Accepted November 12, 2024

The paper presents the results of an experimental study of the interaction of a supersonic flow behind an incident shock wave with a cylindrical obstacle and a boundary layer developing on the inner surface of a driven section of the rectangular shock tube. It is shown that this approach allows one to study the features of non-stationary heat transfer in the front separation region at a supersonic flow enthalpy of  $\approx 3$  MJ/kg and a stagnation temperature of  $\approx 2500$  K. Spatial and temporal distributions of pressure and heat flux in the front separation region are obtained. The structure and dynamics of the interaction region are studied using shadow photography.

**Keywords:** shock tube, shadow photography, heat flux, boundary layer, shock wave, viscous-inviscid interaction, horseshoe vortices.

DOI: 10.61011/TP.2024.12.60430.309-24

### Introduction

Despite the long history of investigation, the problem of shock waves and boundary layer interaction remains relevant and critical in experimental and computational gas dynamics research, which has both fundamental and applied significance [1–5]. Of considerable interest is the study of the flow near a rectangular protuberance [6–8], a cylinder [9–12], and a blunted fin [13–15] located on a plate, since they simulate the characteristic elements fixed on the surface of a high-speed aircraft. These configurations are distinguished by a fundamental three-dimensional flow pattern with a complex shock wave structure, accompanied by separation and attachment of the boundary layer [6–15]. This leads to a strong spatial inhomogeneity of the pressure field and heat flux over the surface of the plate itself and the obstacle. This is most evidently manifested near the junction, where regions with extremely high values occur, exceeding by an order the magnitude in the undisturbed boundary layer. In practice, these effects are often undesirable, since increased mechanical and thermal loads can lead to the destruction of the thermal protective coating and further the entire aircraft itself [17].

So far, the basic physical mechanisms that determine the viscous-inviscid interaction in a wide range of Mach and Reynolds numbers of supersonic flow have been studied in details, theoretically and experimentally [16,17]. The vast majority of experimental work has been performed in the long duration wind tunnels. They allow generating a supersonic flow with parameters controlled with high precision. Among typical diagnostics methods are measurements of pressure on the plate surface and on

the obstacle surface, visualization of the current flow by various methods such as shadow photography [8,11,12], PIV-method and oil-black streamline tracing [11,14]. Heat fluxes are measured much less frequently [6–8,14], as well as visualization of thermal fields using thermal sensitive paints [13,17]. Such experiments are primarily intended for obtaining the time-averaged values in the field of viscous-inviscid interaction at a required spatial resolution. High reliability of such experimental data makes it possible to consider them as reference data and apply, in particular, to verify the numerical computations [18].

An important area of modern research is the analysis of unsteady flow characteristics aimed at studying the mechanisms of formation of flow instability [1–5]. The main interest is the dynamics of the separation region as a whole [12,14], pulsation characteristics of pressure on the plate's and obstacle's surface [12,14], spatial energy spectra of pressure pulsations and their correlations [5,12]. It should be noted that the bulk of experimental data on non-stationary characteristics was obtained based on the analysis of pressure measurements, while the number of studies describing the heat fluxes diagnostics in the separation region is currently insignificant.

A significant limitation when using the long duration gasdynamic facilities installations is the incomplete correspondence of experimental conditions to real high-speed flight. This does not allow us to fully investigate the effect of gas properties at high temperatures and reproduce the aerothermodynamics of the supersonic flow. This problem can be solved only using high-enthalpy gasdynamic facilities [19,20]. As a rule, such studies are carried out on reflected shock tubes [6–8,21], however, in this case, it is not

a trivial task to reliably determine all parameters of the gas flow at the nozzle outlet [22]. The issue of non-stationary and pulsation flow characteristics is also difficult, given that the test time is often comparable to the typical oscillation time in the separation region.

A potential approach, when it is possible to partially reproduce the impact of high-temperature effects, is to place an obstacle on the inner surface of the shock tube driven section [23]. In this case, it acts as a plate along which the boundary layer develops, and the obstacle is wrapped by a supersonic flow behind the incident shock wave. Within the framework of this approach, the parameters of supersonic flow can be determined with sufficient accuracy according to the initial experimental conditions, while the level of disturbances is lower than when using reflected shock tubes; however, the range of achievable gas dynamic parameters becomes noticeably smaller, in particular, the maximum Mach number is limited due to the strong heating of gas downstream the incident shock wave when the enthalpy of supersonic flow is sufficiently high. It is also necessary to take into account the transverse inhomogeneity and time variation of the flow parameters at the measuring point due to deceleration of the incident shock wave caused by the boundary layer formation on the inner surface of the driven section [24].

This paper presents the results of an experimental study of the interaction of a supersonic flow downstream the incident shock wave with a cylindrical obstacle installed across the driven section of a rectangular shock tube. Using the shadow photography method, the structure and dynamics of the region of viscous-inviscid interaction near the cylinder are investigated. The pressure and heat flux along the symmetry line upstream the cylinder were measured. The spatial and temporal distribution of the average values of these magnitudes is obtained. Significant pulsations of the heat flux have been recorded at short distances from the lateral surface of the cylinder in the turbulent phase of the flow. This study is different from [23] in that the enthalpy of supersonic flow and the deceleration temperature are a way higher, and, consequently, the real properties of the test gas at high temperatures are observed as more distinct.

Despite the above limitations, the results show that this approach makes it possible to study the features of the viscous-inviscid interaction in the front separation region in a certain range of Mach and Reynolds numbers when the enthalpy of supersonic flow is  $\approx 3\text{MJ/kg}$  and stagnation temperature reaches  $\approx 2500\text{K}$ , which is practically unachievable in the long duration gasdynamic facilities built according to the Ludwig scheme; thus, this approach can be used along with the reflected shock tubes.

## 1. Experimental setup

The experiments were carried out on a rectangular-section shock tube at Ioffe Physical-Technical Institute. The length

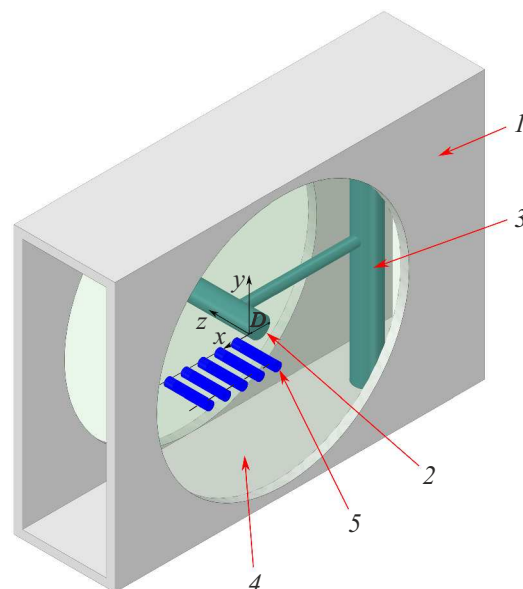


**Figure 1.** Fragment of the shock tube driven section 1 with a cylinder 2 installed in the holder 3. Either a glass window 4, can be installed in the side wall, or a metal plug with pressure sensors 5 or a heat flux sensor.

of the driver section is 1.08 m, the length of the driven section is 10 m, the channel is 150 mm in height and 50 mm in width. The sections are separated by a diaphragms unit equipped with vertical knife. This makes it possible to achieve high repeatability of pressure in the driven section with the diaphragm opening, and, accordingly, repeatability of the Mach number of the incident wave and parameters of the supersonic flow downstream this shock wave. A horizontal cylinder with a diameter of  $D = 12\text{mm}$  was installed in the driven section at a distance of 8.6 m from the diaphragm block with a side surface facing the flow. The cylinder was mounted on a horizontal pin 92 mm long resting on a vertical holder with a diameter of 15 mm (Fig. 1).

There are windows in the side walls of the driven section for optical monitoring of the flow at the point of cylinder installation. Such system is assembled on the base of IAB-451 device. Two lighting and photo-detection systems were used in these experiments. In the first case, a semiconductor laser with electron beam pumping and a pulse duration of 10 ns was used together with a digital SLR camera. It was used to obtain single shadow photos with a resolution of  $4912 \times 3264$  pixels. The spatial resolution, limited by the capabilities of the shadowgraph equipment, was  $\sim 0.1\text{mm}$ . This made it possible to analyze the spatial structure of the area of viscous-inviscid interaction at fixed points of time. In the second case they used Luminus CBT-120-G LED and a multi-frame high-speed camera Revealer X213. The developed LED power supply scheme made it possible to create a series of identical current pulses with an amplitude of up to 250 A, duration of up to  $2\mu\text{s}$  and an interval

between them  $20\ \mu\text{s}$ . In each experiment, at least 60 photos with a resolution of  $704 \times 264$  pixels were obtained. This made it possible to analyze the dynamics of interaction during the entire test time. The spatial resolution, limited by the capabilities of a high-speed camera, was  $\sim 0.25\ \text{mm}$ .

In addition to optical diagnostics, pressure measurements were carried out at various distances from the side surface of the cylinder. To do this, instead of one of the windows, an identical-sized plug with five PCB Piezotronics 113B28 pressure sensors was installed. They were installed along a line passing through the center of the cylinder and parallel to the axis of symmetry of the shock tube; the distance between the centers of neighboring sensors was 12 mm. Upper limit of the detected frequencies was  $\sim 100\ \text{kHz}$ , frequency of the sensor eigen oscillations was  $> 500\ \text{kHz}$ . Electrical signals were recorded using a digital oscilloscope with a time resolution of  $1\ \mu\text{s}$ . Since the sensors' working surface is 5.5 mm in diameter, the spatial resolution does not exceed  $\sim D/2$ , which limited the possibility of obtaining a detailed pressure distribution in the front separation region.

To measure the heat flux, a similar plug was made with a sensor on an anisotropic thermocouple made of bismuth single crystal [25,26], mounted in a replaceable insert (Fig. 2). Each thermoelement had a length of 4 mm, a width — 0.4 mm, and thickness — 0.35 mm. During installation, the insert was oriented so that the long side of the thermocouple was positioned vertically, across the gas flow. Thus, the spatial resolution in the horizontal direction was  $\sim 0.4\ \text{mm}$ . The heat flux detection in the undisturbed boundary layer without a cylinder showed that maximum amplitude of the sensor signal in the selected gasdynamic mode is  $\sim 1\ \text{mV}$  and corresponds to the lower limit of measurements of the digital oscilloscope used. Therefore, in order to increase the signal-to-noise ratio and improve the quality of mea-



**Figure 2.** Insert with heat flux sensor on an anisotropic thermoelectric element made of single-crystal bismuth.

surements, the sensor was connected to an intermediate amplifier based on INA128 instrument amplifier. The gain coefficient was  $\times 200$  or  $\times 500$  depending on the maximal signal amplitude. The signal was detected using a digital oscilloscope with a temporal resolution of  $0.4\ \mu\text{s}$ . The heat flux was calculated from an electrical signal using the technique described in [27]. Before conducting the experiments, the sensor was calibrated using a reflected shock wave [28]. The uncertainty of the volt-watt coefficient and the calculated heat flux did not exceed 10%.

When measuring at short distances from the side surface of the cylinder, a gradual decrease in the dynamic characteristics of the sensor was detected in the region of maximum heat flux values. The analysis showed that this is caused by the destruction of bismuth single-crystal structure near the working surface of the heat flux sensor and by formation of a thin layer that is not involved in the generation of thermal EMF [29]. To restore the sensor's ability to detect the high-frequency components of the heat flux, its working surface was ground with a P2500 grit sandpaper before each test. A control calibration based on the reflected shock wave was also periodically performed to check the volt-watt coefficient.

Since the position of the cylinder and sensors in the plug is unchanged in each experiment, a series of experiments were conducted with identical initial conditions, but with different distances from the side surface of the cylinder to the measuring points, in order to obtain a spatial distribution of pressure and heat flux. The applicability of this approach is based on the high reproducibility of experimental conditions both in terms of diaphragm rupture pressure and flow structure in the field of viscous-inviscid interaction. For this purpose, special attention was paid to the accuracy of glass windows and sensor plugs installation to minimize disturbances in the boundary layer due to the possible mismatch of their plane with the inner surface of the driven section.

It should be emphasized that the flow pattern of the cylinder during the test time is not fully stationary. The parameters of the supersonic flow at the measuring point change over time due to the deceleration of the incident shock wave caused by formation of a boundary layer on the inner surface of the shock-tube driven section. The bow shock wave also interacts with the boundary layer to form a  $\lambda$  structure, which can affect its shape and position. The cylinder diameter, the parameters of the driver and driven gas were selected based on the required Reynolds number, as well as the possibility of implementing „quasi-stationary“ flow of maximum duration with minimal variations in the flow parameters. To evaluate this change the extent of moving away and the shape of the front shock wave was used as a criterion, where the change of the wave was detected by using shadow photography and laser illumination with an accuracy of  $\approx 0.1\ \text{mm}$ .

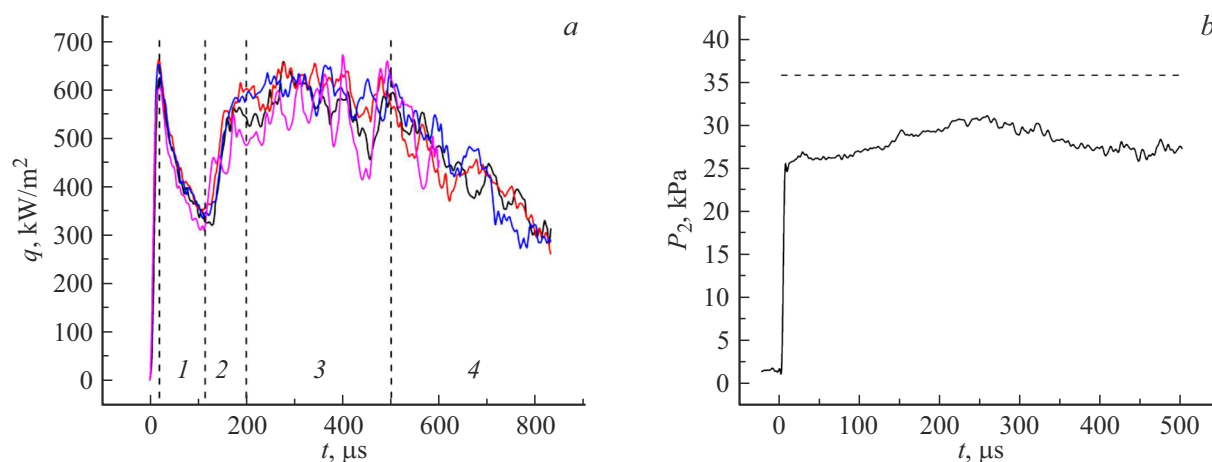


**Figure 3.** Heat flux on the interior surface of the driven section after passing of the incident shock wave (*a*), where 1 — laminar phase, 2 — laminar-turbulence layer transition, 3 — turbulence phase, 4 — motion of pushing gas; static pressure downstream the incident shock wave (*b*), experimentally measured (solid line) and calculated based in the input experimental data (dashed line).

## 2. Supersonic flow downstream the incident shock wave

In the first series of experiments, the pressure and heat flux in the boundary layer were recorded without an installed cylinder. The main tasks were to analyze the duration and variation of parameters of the supersonic flow during the test time of the shock tube in the selected mode. The effect of the sensor plug installation precision on evolution of disturbances in the boundary layer and the repeatability of experiments was also investigated. The latter is fundamentally important, since in each experiment measurements were carried out at only one point, and spatial distributions were obtained by moving the cylinder relative to stationary sensors, accompanied by removing and installing the plug. Another important task was to analyze the applicability of the sensor–amplifier assembly for detecting high-frequency oscillations of the heat flux at short distances from the cylinder’s side surface.

Helium was used as a driver gas, air was used as an test gas. Fixed pressure of the diaphragm opening in the drive section  $p_4 = 810 \pm 20$  kPa. Initial pressure in the driven section was measured by InstruTech CVG101 sensor and was  $P_1 = 1.33 \pm 0.3$  kPa. The measured Mach number of the incident shock wave near the location of the cylinder was  $M_1 = 4.75 \pm 0.1$ .

Fig. 3, *a* illustrates the results of measuring the heat flux obtained in different experiments. The moment when the incident shock wave passes by the sensor is taken as zero. Four characteristic sections can be distinguished on the curve, corresponding to the laminar (1), transitional (2) and the turbulent phase of the flow (3), as well as the movement of the cold driver gas (4). In the first phase, after a drastic growth, the heat flux decreases by a factor of  $\sim 1/\sqrt{t}$ , which is caused by an increase in the thickness of the laminar boundary layer. Further, at time  $t \approx 120$   $\mu$ s, corresponding to the Reynolds number  $Re = 3.3 \cdot 10^5$ , the

heat flux rises drastically due to transition to a turbulent flow condition. At time  $t \approx 600$   $\mu$ s, corresponding to the Reynolds number  $Re = 1.7 \cdot 10^6$ , a noticeable decrease in the heat flux begins, caused by the arrival of a cold driver gas at the measuring point. Thus, it can be assumed that the maximum test time in this mode does not exceed 500  $\mu$ s. Average value of the heat flux in the turbulent phase amounts to 400–600 kW/m<sup>2</sup>.

The coincidence of the onset of the laminar-turbulent transition in various experiments indicates that the plug has been installed with high precision, and, accordingly, that no any noticeable boundary layer disturbances were observed. The close average values of the heat flux and the duration of each phase practically coincide, which indicates a good repeatability of the initial experimental conditions, and, accordingly, the air flow parameters downstream the incident shock wave. It should be noted that the level of oscillations in the turbulent phase increases over time. In case of experiments with an installed cylinder, the presence of a separation region leads to an additional disturbance of the flow and lower duration of the laminar and transition phase. For this reason, the phase durations shown in Fig. 3, *a* should be considered as upper-bound estimates.

Fig. 3, *b* illustrates the measured pressure  $P_2$  downstream the incident shock wave and the theoretical value calculated based on initial pressure in the driven section  $P_1$  and measured Mach number  $M_1$  (see the Table) using NenzfId tool in Gas Dynamics Toolkit (GDTK) [30]. The non-monotonic profile of the curve is caused by an incident shock wave’s formation and acceleration area near the diaphragm unit and an area of its further deceleration caused by a boundary layer formation on the inner surface of the driven section[31,32]. A noticeable discrepancy between the experimental and theoretical values can be caused by a sufficiently high uncertainty of the initial pressure measurement  $P_1$ , amounting to  $\pm 10\%$  of the measured value. From experience of working with this shock tube,

**Table 1.** Calculated parameters of supersonic air flow downstream the incident shock wave

Density $\rho_2$ , kg/m <sup>3</sup>	0.086
Temperature $T_2$ , K	1439
Pressure $P_2$ , Pa	35700
Heat capacity $C_{p2}$ , J/(kg·K)	1214
Specific enthalpy $H_2$ , J/kg	$2.8 \cdot 10^6$
Viscosity $\mu_2$ , Pa·s	$5.4 \cdot 10^{-5}$
Speed $V_2$ , m/s	1330
Mach number $M_2$	1.8
Single Reynolds number $Re_2$ , 1/m	$2.1 \cdot 10^6$

it is known that the measured Mach number at the end of the driven section is about 10% less than the theoretical value calculated according to the ideal theory. The estimates show that the change in the gas parameters behind the incident wave due to its deceleration is  $\sim 20\%$ , while the Mach and Reynolds numbers change by no more than 5%. From Fig. 3, *b* it can be seen that the test time,  $\approx 500 \mu\text{s}$  relative variation of pressure  $P_2$  doesn't exceed 20% which proves the results of estimates. This makes it possible to consider the supersonic flow past the cylinder as practically unchanged in time.

According to the measurement results [33,34] and theoretical estimates [34,35], in the case of a laminar boundary layer, the heat flux density drops as  $1/\sqrt{t}$ , therefore the value of  $St \cdot Re^{1/2}$  shall be constant. The Stanton and Reynolds numbers are defined as follows:

$$St = \frac{q}{\rho_2 v_2 c_{p2} (T_{aw} - T_w)},$$

$$Re = \frac{\rho_2 v_2^2 t}{\mu_2},$$

where  $T_{aw} = T_2 \left(1 + \sqrt{\text{Pr}} \frac{\gamma-1}{2} M_2^2\right)$ ,  $q$  — density of heat flux,  $T_w$  — temperature of interior wall of the shock tube driven section,  $\text{Pr}$  — Prandtl number  $\gamma$  — adiabatic index. According to [34], the value  $St \cdot Re^{1/2} = 0.66$ , in these experiments  $St \cdot Re^{1/2} = 0.80 \pm 0.04$  was obtained (Fig. 4, *a*). This difference may be due to the uncertainty of the initial experimental data.

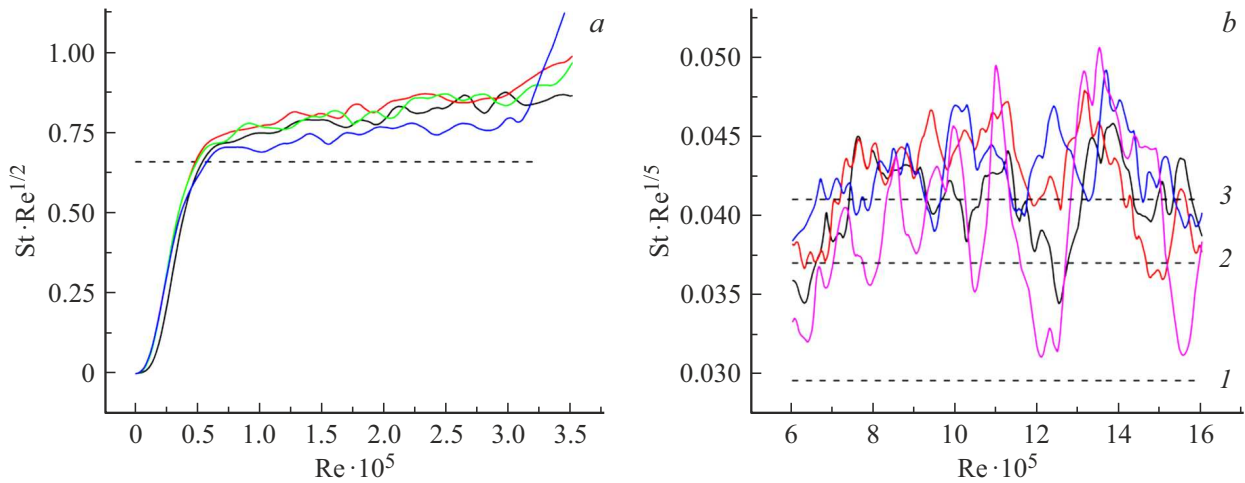
Heat transfer in a developed turbulent boundary layer is described by the ratio  $St \cdot Re^{1/5} = \text{const}$ . In the considered studies [33–35], with which the results of the present experiments were compared, the value of constant  $St \cdot Re^{1/5}$  lay within 0.0296–0.041. The value of the constant in these experiments obtained as a result of averaging over the range of Reynolds numbers  $Re = 5 \cdot 10^5 - 16 \cdot 10^5$ , was  $St \cdot Re^{1/5} = 0.039 \pm 0.003$  (Fig. 4, *b*). Insufficient change in the products of  $St \cdot Re^{1/2}$  and  $St \cdot Re^{1/5}$  with time is caused by the use of constant gas parameters (see the Table).

### 3. Flow structure near the cylinder

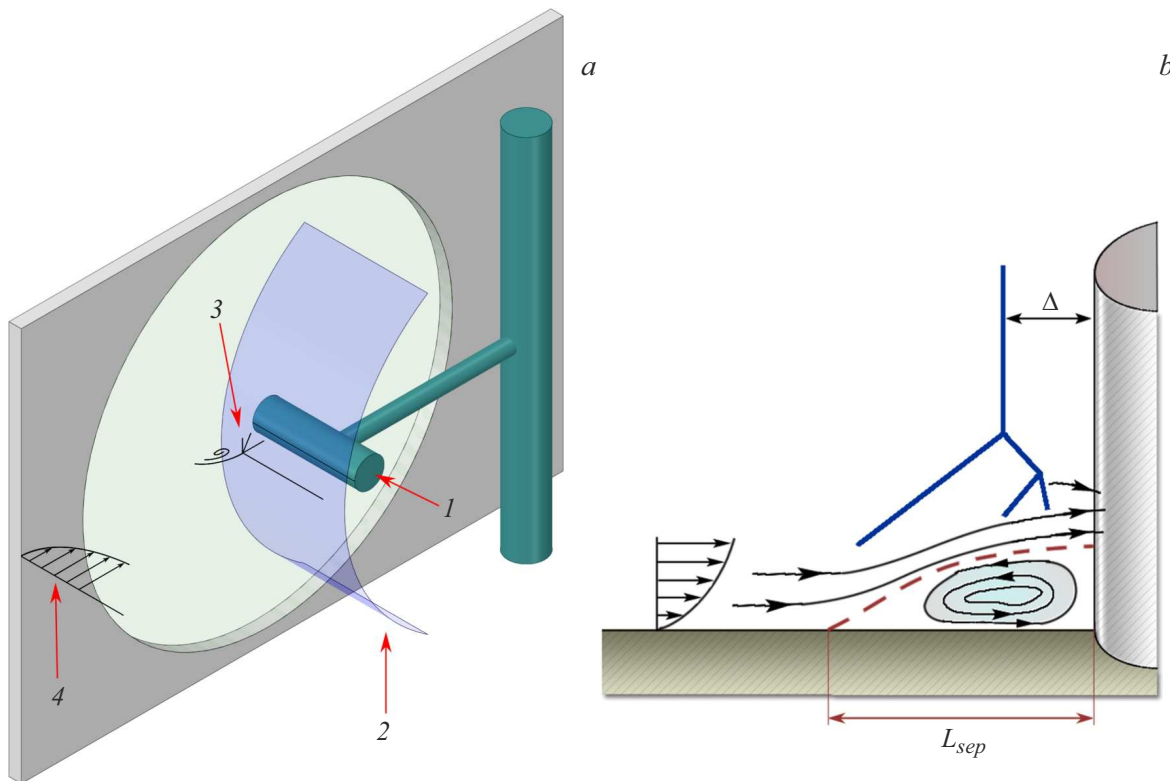
In the second series of experiments, the flow structure in the front separation region was studied using shadow photography. After the incident shock wave passes through and the supersonic flow begins to flow around the cylinder, a bow shock wave is formed in front of it at a distance of  $\Delta$ . Its interaction with the boundary layer on the inner surface of the driven section leads to the formation of a separation region with horseshoe-shaped vortex structures (fig. 5). It is known [11,36], that the main parameter determining the size of a given area  $L_{sep}$  is the ratio of the cylinder diameter to the thickness of the boundary layer  $D/\delta$ . The studies of parameters [11] show that the ratio  $2 < L_{sep}/D < 3.5$  is valid in a wide range of Mach and Reynolds numbers. At that, a sufficient spread of experimental data used in analysis in paper [11] doesn't allow us speaking of an unambiguous dependence of  $L_{sep}/D$  from  $D/\Delta$ .

Figure 6 shows a series of photographs obtained in one experiment using a high-speed camera. It illustrates the main stages in the development of interaction of the incident shock wave and the following supersonic flow with the cylinder. The photo (Fig. 6, *a*) shows the formation of a bow shock wave  $\hat{1}$  and a localized disturbance region near the critical point 2 caused by its interaction with the boundary layer. Further, the position of the shock wave practically does not change until the flow pattern is disrupted (Fig. 6, *e*), which indicates a slight change in the parameters of the supersonic flow over time, but at the same time the length of the disturbance region along the shock tube axis upstream the shock wave gradually rises. The photo (Fig. 6, *f*) shows destruction of the flow pattern caused by the interaction of the bow shock wave with the boundary layer to form  $\lambda$  configuration and the beginning of the wave motion towards the supersonic flow [35]. The growth of its „thickness“  $3$  is caused by distortion along the optical system axis. It can be seen that starting from  $300 \mu\text{s}$ , the structure of the bow shock wave and the flow near the cylinder begins to change gradually. The gradual disappearance of the visible wave front upstream the disturbance area is caused by an increase in inclination relative to the optical axis and a decrease in the density gradient. The unsteady nature of the structures formed is primarily caused by an increase in the thickness of the boundary layer and the instability of the vortex structures, which leads to a change in the size of the separation region and a slight change in the parameters of the gas flow due to the deceleration of the incident shock wave.

Figure 7 shows a shadow photograph taken at time  $t = 100 \mu\text{s}$  after the incident shock wave came into contact with the side surface of the cylinder 1. The bow wave travel normalized to the cylinder diameter 2, makes  $\Delta/D = 0.67$ . Weak disturbances 3 are visible upstream of it, due to the presence of an extensive separation region. The length of this region along the line of symmetry limited by a weak wave 4 is equal  $L_{sep}/D = 2.25 \pm 0.05$ . There



**Figure 4.** Measured heat fluxes in the boundary layer downstream the incident shock wave with known theoretical dependencies: *a* — laminar flow, dashed line —  $St \cdot Re^{1/2} = 0.66$  [34]; *b* — turbulent flow, dashed line 1 —  $St \cdot Re^{1/5} = 0.0296$  [33], line 2 —  $St \cdot Re^{1/5} = 0.037$  [35], line 3 —  $St \cdot Re^{1/5} = 0.041$  [34].



**Figure 5.** Structure of the current flow in the driven section channel of the shock tube (*a*) and shock-wave structure and position of the separation region (*b*); 1 — cylinder, 2 — bow shock wave, 3 —  $\lambda$ -structure, 4 — profile of the boundary layer on the internal surface of the driven section,  $\Delta$  — standoff distance,  $L_{sep}$  — width of the separation region.

are also disturbances 5 behind the bow wave caused by the formation of horseshoe-shaped vortex structures in the separation region. Analysis of similar shadow photographs obtained every  $20\mu s$ , showed that during  $\sim 300\mu s$ , the standoff distance practically did not increase.

#### 4. Pressure measurement results

In the third series of experiments, pressure and heat flux were measured in the front separation region at various distances from the side surface of the cylinder. The resulting complex structure of the flow leads to a significantly het-

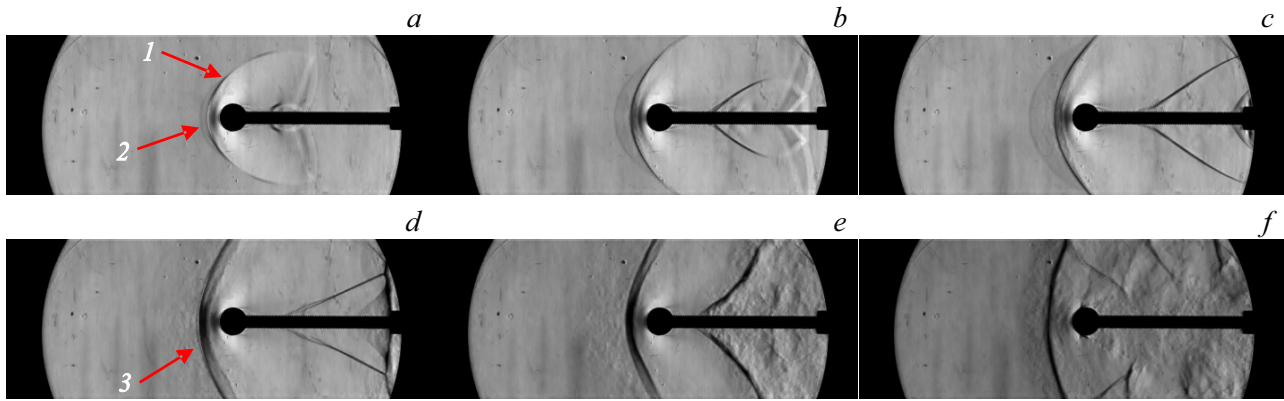


**Figure 6.** Shadow photos in the moment of time from the start of interaction of the incident shock wave with the cylinder side surface: *a* — 20, *b* — 40, *c* — 60, *d* — 140, *e* — 300, *f* — 540  $\mu\text{s}$ ; 1 — formation of bow shock, 2 — formation of disturbances in the critical point, 3 — deformation of the shock wave profile along the optical axis of the shadow photography system.

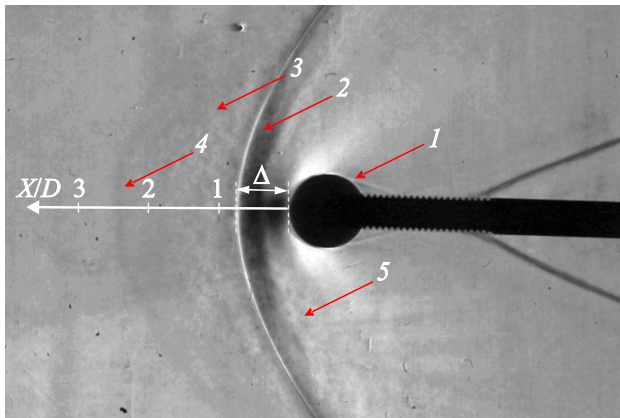


**Figure 7.** Shadow photo of the flow near the cylinder at a moment of time  $t = 100 \mu\text{s}$  after the start of interaction with the incident shock wave. 1 — cylinder, 2 — bow shock, 3 — disturbances in the interaction area, 4 — shock wave upstream the interaction area, 5 — disturbances from the horseshoe-shaped vortices.

erogeneous spatial distribution of gas dynamic parameters. Fig. 8 shows the results of pressure measurement. A drastic increase in the signal of each of the sensors at the initial moment of time corresponds to the passage of an incident shock wave along its working surface. Further, for about  $500 \mu\text{s}$ , the average pressure value remains almost unchanged, despite the change in the flow structure (Fig. 6). It can be seen that noticeable oscillations are observed on the signals of sensors installed within the front separation region at a distance of  $x/D < 2.75$ . The maximum amplitude of the oscillations increases as approaching the cylinder, while at short distances from it, the amplitude increases over time. The main reason for this behavior is the unsteady nature of the separation flow itself, caused by its internal instability [12,14]. A similar increase in oscillations is observed over time in the turbulent phase of the undisturbed boundary layer (Fig. 3, *a*). At time

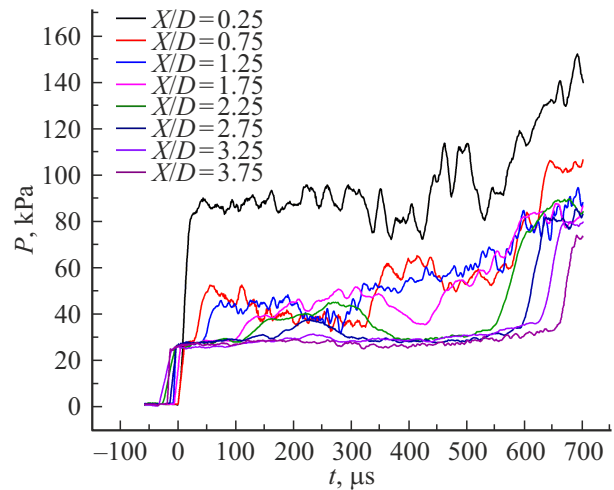


**Figure 8.** Pressure measurement results at various distances from the side surface of the cylinder.

$\approx 600 \mu\text{s}$ , a drastic increase in pressure is observed, which is sequentially recorded by sensors located upstream, which corresponds to the reverse movement of the bow shock due to its interaction with the boundary layer (Fig. 6, *f*). Thus, based on the pressure measurement results, the test time can be estimated as  $500 \mu\text{s}$ .

Figure 9 shows the spatial pressure distribution obtained by averaging over the time interval in  $\pm 25 \mu\text{s}$  in the laminar and transient, as well as turbulent phases of the flow. In both cases, outside the forward separation zone at a distance of  $x/D > 3$ , the value of pressure practically corresponds to the pressure downstream the incident shock wave in an undisturbed flow (Fig. 3, *b*). It can be seen that at the end of the laminar phase, corresponding to the time  $\approx 100 \mu\text{s}$  after the start of the flow and the Reynolds number  $3 \cdot 10^5$ , two characteristic areas of increased pressure are generated near the cylinder. The first area is located directly near the cylinder, and the second — at a distance of  $x/D \approx 1.2$ .

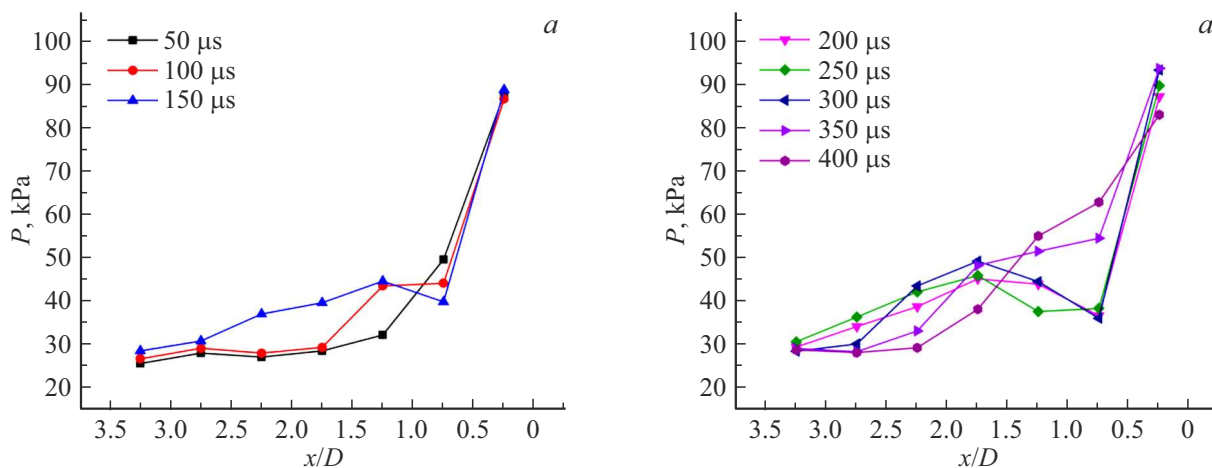


Figure 9. Spatial distribution of the time-averaged pressure values in laminar and transient phases (a) and turbulent (b) phase of flowing.

After the start of the laminar-turbulent transition, the flow structure changes, the shape of the second increased pressure area becomes more pronounced, and it moves away from the cylinder. The maximal value is observed at a distance of  $x/D \approx 1.7$ . Over time, its profile is gradually planed, and a reverse movement towards the cylinder is observed, culminating at time  $400\mu\text{s}$  with formation of a structure with one local maximum. It should be stressed that the results obtained do not allow us to assert that the shape of the observed structures is well-established, and therefore this problem requires further investigation.

### 5. Heat flux measurement results

Figure 10 shows the results of measurements of the heat flux at a distance  $x/D = 0.04$  ( $x = 0.5\text{ mm}$ ) from the cylinder surface to the middle of the heat flux sensor, obtained in a series of four experiments with identical initial conditions. In different experiments the average value differs by no more than 20% and makes  $\sim 4300\text{ kW/m}^2$ , which in practice is an order higher than the level of the heat flux in the undisturbed boundary layer in the turbulence phase of the flow (Fig. 3, a). On two curves, oscillations with a duration of  $50\mu\text{s}$  and an amplitude of about average value of the heat flux are noticeable, occurring in the turbulent phase of the flow, while the amplitude of pulsations on the other curves does not exceed 10%. There are practically no oscillations in the laminar phase. Such a strong difference in the behavior of the heat flux curves indicates a significantly unstable and irregular nature of the flow in the separation zone which is noticeable in the features of the heat transfer process. Similar result was obtained at a distance of  $x/D = 0.12$  ( $x = 1.5\text{ mm}$ ) from the cylinder surface.

It should be noted that a large number of experiments were conducted in this series and heat flux curves with very different levels of oscillations, but with a close average value, were obtained. Analysis of these results showed that this discrepancy is primarily caused by a change in the

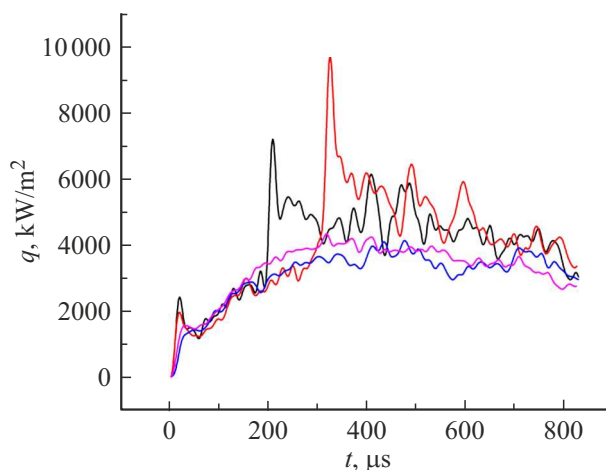
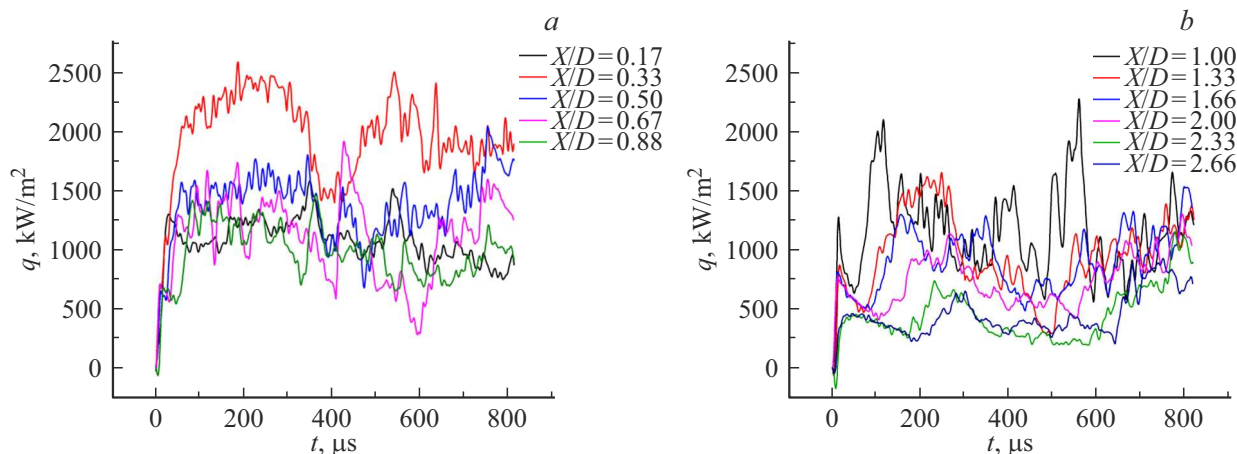


Figure 10. The results of the heat flux measurement at a distance of  $x/D = 0.04$  ( $x = 0.5\text{ mm}$ ) from the cylinder side surface.

dynamic characteristics of the heat flux sensor [29] when measuring high-intensity heat flux in an air environment resulting from the degradation of its operating surface. Since this phenomenon is directly related to non-stationary heat transfer processes and is random in nature, the absence of oscillations on the heat flux curve may be explained by both, their actual absence in the experiment and changes in the surface properties during measurements. However, if they are present, it clearly indicates the presence of such disturbances at the measuring point.

Figure 11 shows the results of heat flux measurements at various distances from the side surface of the cylinder. After a sharp increase in the heat flux at the time of the incident shock wave arrival, a small area of decline corresponding to the laminar flow regime is observed on all curves. A further abrupt increase in the heat flux is due to the arrival of the shock wave reflected from the cylinder and the start of formation of a complex three-dimensional gas dynamic flow structure. At all points at



**Figure 11.** The results of measurements of the heat flux versus time at small (a) and large (b) distances from the cylinder side surface.

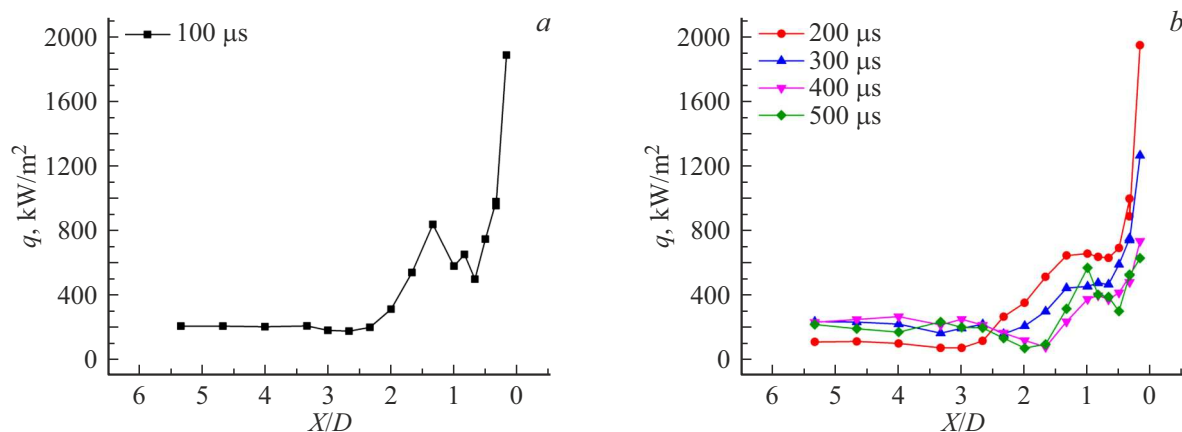


**Figure 12.** Distribution of the heat flux at various distances from the cylinder side surface in the laminar (a) and turbulent (b) flow phases.

distances  $x/D < 0.67$ , the heat flux significantly exceeds the values in the undisturbed boundary layer, the highest value is reached at a distance  $x/D = 0.33$  from the cylinder. Irregular oscillations of various frequencies and amplitudes indicate the unsteady nature of the shock-wave interaction in the region under consideration. The maximum amplitude of heat flux oscillations reaches 50% of the average value over the entire measurement duration. As we move away from the cylinder's side surface, the heat flux oscillations decrease, and the average value tends to the value in the undisturbed boundary layer. At a distance of  $X/D = 2.67$ , which can be considered the boundary of the separation region, the differences are within the measurement error. The localization of the region of maximum heat flux and pressure oscillations near the cylinder side surface (Fig. 8) is caused by the flow structure (Fig. 5,b) and the intensity distribution of turbulent pulsations.

Figure 12 shows the spatial distributions of the heat flux averaged over the  $\pm 25 \mu\text{s}$  interval in the laminar and turbulent phases of the flow. In the first case we may

see the structure similar to the pressure distribution. At a distance of  $x/D < 0.5$ , a local maximum is observed, which is several times higher than the value in the undisturbed boundary layer. The second local maximum which is significantly lower in terms of amplitude is at distance of  $x/D \approx 1.2$ . At distances  $x/D > 2$ , the heat flux level corresponds to the values for an undisturbed boundary layer in the absence of a cylinder. In case of a turbulent boundary layer, two regions of increased heat flux are also observed, but the profile of the second region is much smoother. Over time, there is a decrease in the magnitude of the first maximum and a much more pronounced second maximum is formed which is a characteristic feature arising during the three-dimensional interaction of the shock wave with the boundary layer [2,13,16,23]. At the same time, there is a significant decrease in the size of the separation region, which was also previously experimentally registered in paper [23]. Starting from  $400 \mu\text{s}$ , the local minimum at a distance of  $x/D \approx 1.5$  is observed. It should be noted that when calculating the average values of the heat flux, strong

oscillations at short distances from the cylinder's side surface were not taken into account, since the random nature of their appearance.

## Conclusion

The features of the flow structure in the front separation region in a supersonic flow past a cylindrical obstacle are investigated. This study differs from other experimental studies in that the cylinder was installed on the inner wall of the driven section of the rectangular shock tube, and not on the plate in the supersonic nozzle outlet. In this configuration, a supersonic flow is formed downstream the incident shock wave, and a boundary layer develops along the inner wall of the shock tube. Using shadow photography method, the spatial structure of the area of viscous-inviscid interaction in front of the cylinder and the dynamics of its progress throughout the shock tube test time were determined. The pressure and heat flux were measured in the undisturbed boundary layer and at various distances from the cylinder's side surface.

The obtained results made it possible to analyze the influence of various factors on the test time, during which the flow structure is in the quasi-steady-state, and the reliable measurements are possible. It is shown that, despite the change in the physical parameters of the supersonic flow downstream the incident shock wave, the Mach and Reynolds numbers, which determine the structure of the interaction, remain practically the same.

The results of measuring the heat flux without a cylinder are in good agreement with the known theoretical relationships for laminar and turbulent heat flux. This shows that it is possible to use sensors based on anisotropic bismuth thermoelements for this class of flows, and also proves that the procedure of electric signal calibration and processing is done correctly. It was demonstrated that the heat flux measurement system operation response is sufficient to detect the heat flux oscillations with high frequencies.

The pressure and heat flux were measured at various distances from the cylinder's side surface. Temporal and spatial distributions in the front separation region in the laminar and turbulent phases of the flow are obtained. Two local heat flux maximums are observed. The first one is several times higher than the heat flux in the undisturbed boundary layer. The second, less pronounced maximum, located within  $1 < x/D < 2$ , changes its position during the interaction of the bow shock wave with the boundary layer. Estimates of the size of the front separation region based on thermal measurements correspond to the results of shadow photography diagnostics and pressure measurements. Chaotic fluctuations of the heat flux and pressure of a large amplitude relative to the average value are observed near the cylinder, which is a manifestation of the unsteady nature of the flow in the viscous-inviscid interaction area.

The results obtained show that the approach used, when the obstacle is located on the inner wall of the driven section where the boundary layer evolves downstream the incident shock wave, is a possible way to simulate the interaction of a high-enthalpy supersonic gas flow with the boundary layer. Despite the limitations on the achievable Mach and Reynolds numbers, it makes possible to study the non-stationary heat transfer processes in the front separation region. The presence of pronounced laminar and turbulent phases makes it possible to analyze the features of the flow structure and the distribution of pressure and heat flux at different Reynolds numbers.

## Funding

This study was supported by grant №. 23-29-00286 from the Russian Science Foundation.

## Conflict of interest

The authors declare that they have no conflict of interest.

## References

- [1] D.S. Dolling. *AIAA J.*, **39** (8), 1517 (2001). DOI: 10.2514/2.1476
- [2] H. Babinsky, J. Harvey. *Shock Wave–Boundary–Layer Interactions* (Cambridge University Press, 2011)
- [3] D.G. Gaitonde. *Prog. Aerosp. Sci.*, **72**, 80 (2015). DOI: 10.1016/j.paerosci.2014.09.002
- [4] K. Sabnis, H. Babinsky. *Prog. Aerosp. Sci.*, **143**, 100953 (2023). DOI: 10.1016/j.paerosci.2023.100953
- [5] D.V. Gaitonde, M.C. Adler. *Annu. Rev. Fluid Mech.*, **55**, 291 (2023). DOI: 10.1146/annurev-fluid-120720-022542
- [6] C.S. Kumar, K.P.J. Reddy. *J. Heat Transfer.*, **135**, 121701 (2013). DOI: 10.1115/1.4024667
- [7] C.S. Kumar, T. Singh, K.P.J. Reddy. *Phys. Fluids.*, **26**, 126101 (2014). DOI: 10.1063/1.4902400
- [8] C.S. Kumar, K.P.J. Reddy. *AIAA J.*, **52** (4), 747 (2014). DOI: 10.2514/1.J052658
- [9] D. Gang, S. Yi, L. He. *J. Vis.*, **19**, 581 (2016). DOI: 10.1007/s12650-016-0354-x
- [10] V.Ya. Borovoy, E.G. Zaitsev, V.E. Mosharov, V.N. Radchenko. *Uchenye zapiski TsAGI*, **52** (4), 3 (2021) (in Russian).
- [11] S.A. Lindorfer, C.S. Combs, P.A. Kreth, R.B. Bond, J.D. Schmisser. *Shock Waves.*, **30**, 395 (2020). DOI: 10.1007/s00193-020-00938-z
- [12] C. Combs, P. Kreth, J. Schmisser, E. Lash. *AIAA J.*, **56** (3), 1288 (2018). DOI: 10.2514/1.J056390
- [13] O.R. Tutty, G.T. Roberts, P.H. Schuricht. *J. Fluid Mech.*, **737**, 19 (2013). DOI: 10.1017/jfm.2013.541
- [14] H. Ngoh, J. Poggie. *Phys. Rev. Fluids.*, **7** (2022). DOI: 10.1103/PhysRevFluids.7.093903
- [15] P. Schuricht, G. Roberts. *Proceedings of 8th AIAA International Space Planes and Hypersonic Systems and Technologies Conference, 1998, AIAA Paper 98–1579*. DOI: 10.2514/6.1998-1579
- [16] M. Hemsh, J. Nielsen. *Aerodinamika raket* (Mir, M., 1989) (in Russian).

- [17] V.Ya. Borovoy, I.V. Egorov, V.E. Mosharov, A.S. Skuratov, V.N. Radchenko *Experimentalny nagrev tel v giperzvukovom potoke. Gasodinamicheskie yavleniya i ikh kharakteristiki* (Nauka, M., 2018)
- [18] V.Ya. Borovoy, V.E. Mosharov, A.Yu. Noev, V.N. Radchenko. *Izvestiya RAN. MZhG*, **3**, 58 (2009) (in Russian).
- [19] G. Sangdi, H. Olivier. *Progress in Aerospace Sci.*, **113**, 100607 (2020). DOI: 10.1016/j.paerosci.2020.100607.
- [20] P. Reynier, *Progress in Aerospace Sci.*, **85**, 1 (2016). DOI: 10.1016/j.paerosci.2016.04.002
- [21] S.A. Maszkiewicz, G.I. Gillespie, S.J. Laurence. *Proceedings of AIAA SCITECH Forum, 2022, AIAA Paper 2022-1818*. DOI: 10.2514/6.2022-1818
- [22] G. Sangdi, H. Olivier, C.-Y. Wen. *Phys. Fluids*, **34**, 056103 (2022). DOI: 10.1063/5.0089120
- [23] H. Ozawa, S.J. Laurence. *J. Fluid Mechan.*, **849**, 1009 (2018). DOI: 10.1017/jfm.2018.433
- [24] W. Dagao, G. Han, M. Liu, Z. Li, Z. Jiang. *Phys. Fluids*, **36**, 076125 (2024). DOI: 10.1063/5.0219298
- [25] S.Z. Sapozhnikov, V.Yu. Mityakov, A.V. Mityakov. *Heatmetry: The Science and Practice of Heat Flux Measurement: Heat and Mass Transfer*. (Springer International Publishing, 2020)
- [26] P.A. Popov, N.A. Monakhov, T.A. Lapushkina, S.A. Poniaev. *Tech. Phys.*, **67** (9), 1144 (2022). DOI: 10.21883/TP.2022.09.54677.54-22
- [27] P.A. Popov, S.V. Bobashev, B.I. Reznikov, V.A. Sakharov. *Tech. Phys. Lett.*, **44** (4), 316 (2018). DOI: 10.1134/S1063785018040235
- [28] P.A. Popov, N.A. Monakhov, T.A. Lapushkina, S.A. Poniaev, R.O. Kurakin. *Tech. Phys. Lett.*, **48** (10), 46 (2022). DOI: 10.21883/TPL.2022.10.54798.19297
- [29] P.A. Popov, A.V. Masyukevich, E.V. Kolesnikov, A.B. Podlaskin. *Pis'ma v ZhTF*, **50** (12), 36 (2024) (in Russian). DOI: 10.61011/PJTF.2024.12.58063.19882
- [30] Electronic source. GDTk — a collection of software for doing gas dynamics, from simple desktop calculations through to simulations on supercomputers. Available at: <https://gdtk.uqcloud.net> (Date of access 02/10/2024)
- [31] T.V. Bazhenova, L.G. Gvozdeva. *Nestazionarniye vzaimod-eistvia udarnykh voln* (Nauka, M., 1977) (in Russian).
- [32] S. Janardhanraj, K. Abhishek, G. Jagadeesh. *J. Fluid Mech.*, **910** (A3), 1 (2021). DOI: 10.1017/jfm.2020.914
- [33] W.R. Davies, L. Bernstein. *J. Fluid Mech.*, **36** (1), 87 (1969). DOI: 10.1017/S0022112069001534
- [34] H. Knauss, T. Roediger, D. Bountin, B. Smorodsky, A. Maslov, J. Srulijes. *J. Spacecr. Rockets*, **46** (2), 255 (2009). DOI: 10.2514/1.32011
- [35] R.A. Hartunian, A.L. Russo, P.V. Marrone. *J. Aeronautical Sci.*, **27** (8), 587 (1960). DOI: 10.2514/8.8656
- [36] V.Ya. Borovoi, M.V. Ryzhkova. *Izv. AN SSSR. MZhG*, **1**, 78-87 (1974) (in Russian).

*Translated by T.Zorina*

*Translated by T.Zorina*